PROCEEDINGS OF SCIENCE

# Search for a light charged Higgs boson decaying into $c\bar{s}$ at CMS

**Gouranga Kole**[*†]
*Tata Institute of Fundamental Research*
*Homi Bhabha Road, Colaba*
*Mumbai 400005, India*
*E-mail:* gouranga@tifr.res.in

We present results on the search for a light charged Higgs boson that can be produced in the decay of a top quark and later decays into a charm and an antistrange quark. The analysis is performed using 19.7 $\text{fb}^{-1}$ pp collison data recorded with the CMS detector at LHC.

*Prospects for Charged Higgs Discovery at Colliders - CHARGED 2014,*
*16-18 September 2014*
*Uppsala University, Sweden*

[*]Speaker.
[†]On behalf of the CMS Collaboration

 

PoS(Charged2014)013

## 1. Introduction

A Higgs boson has recently been discovered by ATLAS [1] and CMS [2] with a mass close to 125 GeV and properties, within uncertainties of the available data, consistent with those expected from the standard model (SM). Although this would complete the SM, still the latter cannot be the full story having many missing links such as dark matter, baryon asymmetry and gravity. Several extensions to the SM have been proposed to address these inconsistent features. The minimal supersymmetric standard model (MSSM) is one such model that contains two Higgs doublets, resulting in five physical Higgs states: a light and heavy *CP*-even $h$ and $H$, a *CP*-odd $A$, and two charged Higgs bosons $H^{\pm}$. At tree level, the MSSM Higgs sector can be expressed in terms of two parameters, which are usually chosen to be the mass of the *CP*-odd Higgs boson ($m_A$) and the ratio of the vacuum expectation values of the two Higgs doublets ($\tan\beta$).

The lower limit on the charged Higgs boson mass is 78.6 GeV, as determined by LEP experiments [3, 4]. If the mass of the charged Higgs boson is smaller than the mass difference between the top and the bottom quarks, the top can decay via $t \to H^+ b$. For $\tan\beta < 1$, the charged Higgs boson preferentially decays to a charm and an antistrange quark ($c\bar{s}$). In the two Higgs doublet model of type I and Y the branching fraction $\mathscr{B}(H^+ \to c\bar{s})$ is larger than 10% for any value of $\tan\beta$, while in type II and X it can reach up to 100% for $\tan\beta < 1$ [5]. In this study, we assume $\mathscr{B}(H^+ \to c\bar{s})$ to be 100%. Recently ATLAS has set an upper limit on $\mathscr{B}(t \to H^+ b)$ between 5% and 1% for charged Higgs masses in the range 90-150 GeV [6].

The presence of the $t \to H^+ b$, $H^+ \to c\bar{s}$ decay channel alters the event yield for $t\bar{t}$ pairs having hadronic jets in the final state, compared to the SM prediction. The search for a charged Higgs boson is thus sensitive to the decays of the top pairs $t\bar{t} \to H^{\pm} b W^{\mp} \bar{b}$ and $t\bar{t} \to H^{\pm} b H^{\mp} \bar{b}$, where the charged Higgs boson decays into a charm and an antistrange quark. We perform a model independent search [7] for the charged Higgs boson in the $t\bar{t} \to H^{\pm} b W^{\mp} \bar{b} \to \mu + E_T^{\text{miss}} + \text{jets}$ final state, where the $W$ boson decays to a muon and a neutrino (leading to missing transverse energy $E_T^{\text{miss}}$) and the $H^+$ decays to $c\bar{s}$. The contribution of the process $t\bar{t} \to H^{\pm} b H^{\mp} \bar{b}$ is expected to be negligible in the above final state. Figure 1 shows the dominant Feynman diagrams for this final state both in the SM $t\bar{t}$ process as well as the same in presence of the $H^+$ boson.

## 2. CMS Detector and Object Reconstruction

The distinguishing features of the CMS detector [8] are a 6 m long solenoidal magnet that produces 3.8 T magnetic field, a fully silicon-based tracking device, a $PbWO_4$ crystal electromagnetic calorimeter, a brass-scintilltor sandwich hadron calorimeter, and an excellent muon system. All physics objects used in the analysis are reconstructed with the particle flow (PF) algorithm, essentially combining information from the aforementioned subdectectors. Muons are reconstructed by matching the tracks in the silicon tracker with the hits in the muon system. Jets are reconstructed based on the anti-$k_T$ algorithm with a cone radius parameter $R = 0.5$. The $E_T^{\text{miss}}$ is defined as the negative vector sum of the transverse momenta ($p_T$) of all PF candidates. To identify jets originating from a $b$ quark, we apply the $b$-jet identification criteria that involve the use of secondary vertices together with track-based lifetime information.


**Figure 1:** Leading-order Feynman diagrams for (left) the SM $t\bar{t}$ production at LHC in the muon final state, and (right) the same in presence of the charged Higgs boson [7].

## 3. Backgrounds

Different backgrounds such as $t\bar{t}$, $W$+jets and $Z$+jets are generated with Madgraph 5 [9] interfaced with Pythia 6.4 [10]. The UE tuning Z2* [11] and CTEQ6M [12] PDFs are used. The $t\bar{t}$ events are estimated from the next-to-next-to-leading-order (NNLO) SM prediction with a production cross section of $245.8 \pm 6.0$ pb. The single top processes are calculated using Powheg [13]. The $W$+jets background is calculated at NNLO with FEWZ3.1 [14], while $Z$+jets and single top events are also normalized to NNLO cross-section calculations. The signal $t\bar{t} \to H^{\pm}bW^{\mp}\bar{b}$ sample is generated with Pythia 6.4 and normalized using the same production cross section as the SM $t\bar{t}$. The cross sections of diboson backgrounds ($WW$, $WZ$ and $ZZ$) are computed with MCFM [15].

## 4. Event Selection and Analysis

We select events with a well-identified muon having $p_T > 25$ GeV and pseudorapidity $|\eta| < 2.1$. The muon is required to be isolated from the surrounding hadronic activity by imposing a PF-based relative isolation criterion, $I_{rel} < 0.12$ [7]. Any event that contains an additional muon or electron with $p_T > 10$ GeV and $|\eta| < 2.5$ passing a loose isolation requirement, $I_{rel} < 0.3$, is rejected. For a consistent data-MC matching, the trigger, muon ID and isolation scale factors are applied to MC events as a function of muon $p_T$ and $\eta$. These scale factors are derived using a tag and probe technique based on $Z \to \mu\mu$ events. Events are required to have at least four jets with $p_T > 30$ GeV and $|\eta| < 2.5$, where two of them arise from top quarks and the other two from $W/H^{\pm}$ boson. Owing to the missing neutrino in the final state, we require the event to have $E_T^{\text{miss}} > 20$ GeV. This criterion also helps in suppressing the QCD multijet and $Z$+jets backgrounds, where there is no real source of $E_T^{\text{miss}}$. A kinematic fit is used to reconstruct $t\bar{t}$ events from the final states resulting in an improved mass resolution for the hadronically decaying boson. This fit constrains the event to the hypothesis for a production of two top quarks, each one decaying to a $W$ boson and a $b$ quark. As indicated above, one of the $W$ bosons decays into a muon-neutrino pair, while the other boson ($W$ in SM $t\bar{t}$ or $H^+$ for the signal) decays into a quark-antiquark pair. As we are interested

in the reconstruction of the $W/H^+$ boson mass, we constrain the reconstructed mass of the two top quarks to 172.5 GeV in the fit. Only jets passing the $b$-tagging requirement are considered as candidates for the $b$ quarks in the $t\bar{t}$ hypothesis, while all other jets are considered as candidates for the light quarks in the boson's hadronic decay. For each event, the assignment that gives the best fit probability is finally retained. As the top $p_T$ spectrum is found to be softer in simuations compared to the data, we reweight the $t\bar{t}$ MC events according to the scale factors derived based on Ref. [16].

Figure 2 (left) shows the $W$ and $H^+$ boson mass distributions obtained from the kinematic fit after full event selection with MC simulated samples. As evident from the plot, the kinematic fit significantly improves the dijet mass resolution, which is crucial in separating the $H^+$ from the $W$ peak. Figure 2 (right) shows the transverse mass ($m_T$) distribution of the system comprising the muon and $E_T^{\text{miss}}$, which shows a good agreement between data and expected SM background from MC simulations.

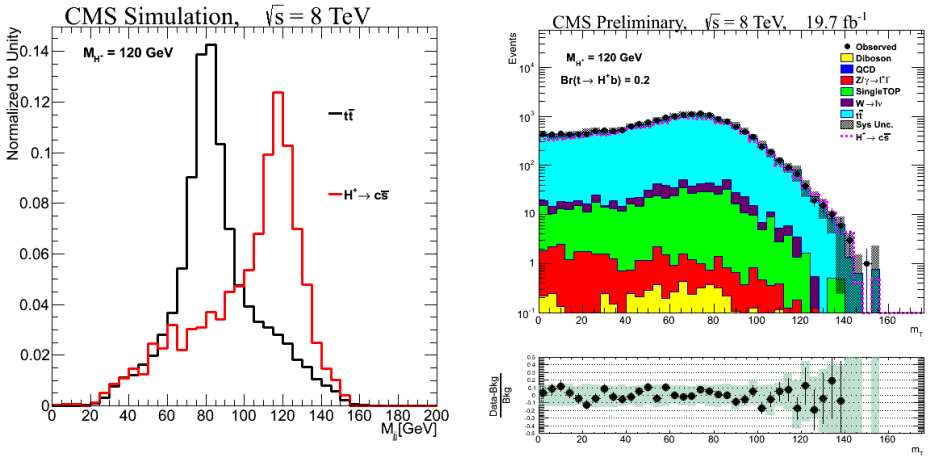


**Figure 2:** (Left) Invariant mass distributions of the dijet system decaying to $c\bar{s}$ obtained from a kinematic fit for the SM $t\bar{t}$ events and the same in the presence of $H^+$ ($m_H = 120\,\text{GeV}$) after all selections with MC simulated samples. (Right) the $m_T$ distribution after the kinematic fit and all other selections [7].

## 5. Systematic Uncertainties

The uncertainty in the jet energy scale (JES) is the leading source of systematic uncertainty in this analysis, since we are using the dijet mass as the final discriminator. It is estimated as a function of the jet $p_T$ and $\eta$ according to Ref. [17], and is then propagated to $E_T^{\text{miss}}$. The uncertainty in JES changes both the event yield and shape of the dijet ($W$ or $H^+$) mass distribution. To estimate the uncertainty in the dijet mass distribution, the jet momenta are scaled according to the JES uncertainty by $\pm 1\sigma$. The difference in the dijet shape used as a shape uncertainty in the limit calculation. The uncertainty in $b$-tagging efficiency and light-jet misidentification probability is another major source of uncertainty, as our selection requires two $b$-tagged jets. The theoretical uncertainties on the cross sections of various processes are also considered. The uncertainty in the production cross section of the $t\bar{t}$ process, which is common to both SM $t\bar{t}$ and signal channel, is an

important source of uncertainty. The uncertainty due to the variation of renormalization and factorization scales used in $t\bar{t}$ simulations is studied by simultaneously changing the nominal scale values by factors of 0.5 and 2.0. An additional shape nuisance is also taken into account as the uncertainty due to matching thresholds used for interfacing the matrix elements generated with Madgraph and Pythia parton showering. The thresholds are changed from the default value of 20 GeV down (up) to 10 (40) GeV. Other bin-by-bin uncertainties are also applied to all backgrounds. Further, a nuisance parameter corresponding to the uncertainty in the top $p_T$ reweighting is considered. Finally, the uncertainty in the integrated luminosity is estimated to be 2.6%.

## 6. Results and Summary

The event yields after all selections are listed in Table 1 along with their statistical and systematic uncertainties. The expected number of signal events from the $t\bar{t} \to H^{\pm}bW^{\mp}\bar{b}$ ($HW$) process for $\mathscr{B}(t \to H^+b) = 20\%$ is also presented in the table. Assuming that any excess or deficit of

**Table 1:** Expected signal and background events are provided with their statistical and systematic uncertainties. The number of events observed in the 19.7 $\text{fb}^{-1}$ of data is also presented.

| Source | $N_{events} \pm$ uncertainty |
|---|---|
| $HW$, $M_H = 120$ GeV, $\mathscr{B}(t \to bH^+) = 20\%$ | $3670 \pm 503$ |
| SM $t\bar{t}$ | $16911 \pm 2163$ |
| $W$+jets | $242 \pm 52$ |
| $Z$+jets | $29 \pm 5$ |
| Single top | $463 \pm 50$ |
| Dibosons | $5 \pm 1$ |
| Total background | $17651 \pm 2164$ |
| Data | 17759 |

events in data, when compared with the expected background contribution, is due to the potential signal $t \to H^+b$, $H^+ \to c\bar{s}$ decay, the difference between the observed number of data events and the predicted background contribution ($\Delta N$) can be given as a function of $x = \mathscr{B}(t \to H^+b)$ via:

$$\Delta N = N_{t\bar{t}}^{obs} - N_{t\bar{t}}^{SM} = 2x(1-x)N_{t\bar{t}}^{HW} + [(1-x)^2 - 1]N_{t\bar{t}}^{SM} \tag{6.1}$$

Here, $N_{t\bar{t}}^{HW}$ is estimated from MC simulations forcing the first top quark to decay to $H^{\pm}b$ and the second one to $W^{\mp}b$, and $N_{t\bar{t}}^{SM}$ is also calculated based on simulations, as given by the SM $t\bar{t}$ entry in Table 1. Note that Eq. (6.1) is applicable to any new physics model as there is no explicit dependence on any MSSM parameter. Therefore, our obtained limit in absence of a significant excess or deficit will be model independent in nature.

The LHC-wide CLs method [18, 19] is used to obtain an upper limit on $x = \mathscr{B}(t \to H^+b)$ at the 95% confidence level (CL) using Eq. (6.1). The dijet mass distribution shown in Fig. 3 is used in a binned maximum-likelihood fit to extract a possible signal. The upper limit on $\mathscr{B}(t \to H^+b)$ as a function of $m_{H^+}$ is shown in Fig. 3. The observed limit agrees well with the expected limit within one standard deviation.

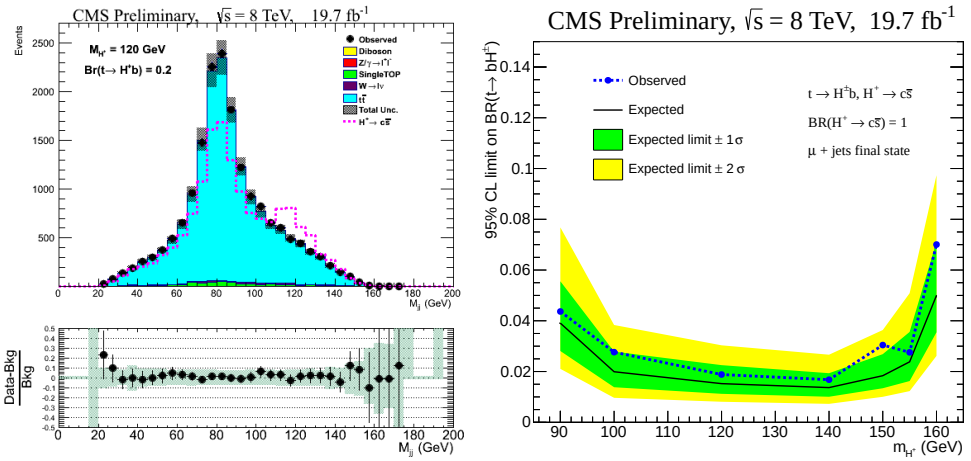


**Figure 3:** (Left) Dijet mass distributions of the hadronically decaying boson after the maximum likelihood fit. (Right) Exclusion limit on $\mathscr{B}(t \to H^+ b)$ as a function of $M_{H^+}$ assuming $\mathscr{B}(H^+ \to c\,\bar{s}) = 100\%$ [7].

A search has been performed for a light charged Higgs boson produced in a top quark decay, subsequently decaying into $c\bar{s}$. The total integrated luminosity of $19.7\,\text{fb}^{-1}$ recorded by CMS at $\sqrt{s} = 8\,\text{TeV}$ are used in the search. In absence of any signal on the dijet invariant mass distribution of the $H^+ \to c\bar{s}$ candidate events, we set a model-independent 95% CL upper limit on the branching fraction $\mathscr{B}(t \to H^+ b)$ assuming $\mathscr{B}(H^+ \to c\bar{s}) = 100\%$. The obtained limits are in the range of $2-7\%$ for a charged Higgs mass between 90 and 160 GeV.

## Acknowledgments

I thank the organizers and CMS collaboration for giving me an opportunity to deliver a talk at this conference.

## References

[1] G. Aad *et al.* (ATLAS Collaboration), Phys. Lett. B **716**, 1 (2012).

[2] S. Chatrchyan *et al.* (CMS Collaboration), Phys. Lett. B **716**, 30 (2012).

[3] P. Achard *et al.* (L3 Collaboration), Phys. Lett. B **575**, 208 (2003).

[4] A. Heister *et al.* (ALEPH Collaboration), Phys. Lett. B **543**, 1 (2002).

[5] M. Aoki, S. Kanemura, K. Tsumura, and K. Yagyu, Phys. Rev. D **84**, 055028 (2011).

[6] G. Aad, *et al.* (ATLAS Collaboration), Phys. J. C **736**, (2013).

[7] CMS Collaboration, CMS-PAS-HIG-13-035, *http://cds.cern.ch/record/1728343*

[8] S. Chatrchyan *et al.* (CMS Collaboration), JINST **3**, S08004 (2008).

[9] J. Alwall *et al.*, JHEP **1106** (2011) 128.

[10] T. Sjostrand, S. Mrenna and P. Z. Skands, JHEP **0605** (2006) 026.

[11] S. Chatrchyan *et al.* (CMS Collaboration), JHEP **1109** (2011) 109.

[12] J. Pumplin *et al.*, JHEP **0207** (2002) 012.

[13] S. Alioli, P. Nason, C. Oleari and E. Re, JHEP **0909** (2009) 111; E. Re, Eur. Phys. J. C **71** (2011) 1547.

[14] Y. Li and F. Petriello, Phys. Rev. D **86** (2012) 094034.

[15] N. Kidonakis, arXiv:1205.3453 [hep-ph].

[16] CMS Collaboration, CMS-PAS-TOP-12-027, *http://cds.cern.ch/record/1523611*

[17] S. Chatrchyan *et al.* (CMS Collaboration), JINST **6**, P11002 (2011).

[18] L. Read, J. Phys. G: Nucl. Part. Phys., **28** (2002) 2693.

[19] T. Junk, Nucl. Instrum. Meth. A, **434** (1999) 435.